Distorted and inequivalently charged C_{60} anions in $Yb_{2.75}C_{60}$

P. H. Citrin, E. Özdaş,* S. Schuppler,† A. R. Kortan, and K. B. Lyons‡
Bell Laboratories, Lucent Technologies, Murray Hill, New Jersey 07974
(Received 28 January 1997)

Near-edge x-ray absorption measurements from single-phase $Yb_{2.75}C_{60}$ establish that all of the Yb cations are divalent, meaning that the average negative formal charge of the C_{60} anions is 5.5. Extended x-ray absorption fine structure (EXAFS) and Raman measurements also reveal that the C_{60} anions are distorted in shape, despite their well-ordered local structure around the Yb cations. These findings are combined with a model to show that the charge transferred from Yb to C_{60} is both anisotropically distributed on the anions and inequivalently partitioned among them within the unit cell. In the model, the inhomogeneously distributed transferred charge (which arises from the comparatively greater electron affinity of the C_{60} pentagonal faces) interacts strongly with the divalent cations and leads to significant anion distortions. The redistribution of transferred charge is traceable to the three crystallographically different types of C_{60} anions that are surrounded by 8, 10, or 12 Yb cations, a situation similar to the inequivalently coordinated and charged O anions in the high-T_c compound $YBa_2Cu_3O_7$. Additional EXAFS and Raman data from $Yb_{2.75}C_{60}$ heated above 670 °C show the removal of local order around the Yb cations and the production of an amorphous carbidic phase containing Yb(III). Our collective results, along with comparisons to analogous fulleride and organometallic compounds, provide insight into the distinctive structural features of $Yb_{2.75}C_{60}$ and its unique distribution of anion charge. They also have general implications for a variety of other metal-doped fullerides. [S0163-1829(97)03333-X]

I. INTRODUCTION

Electron-donor-intercalated C_{60} fulleride compounds have received much attention because of their extraordinary properties, the most notable of which are the record-high superconducting temperatures for organic systems.[1] Superconductivity has been demonstrated in fulleride compounds doped with monovalent alkali[2] and divalent alkaline-earth metals,[3,4] prompting explorations with predominantly trivalent rare-earth metals. A single-phase Yb fulleride, which becomes superconducting below 6 K,[5] has recently been prepared, followed shortly by the report of a Sm fulleride[6] with a presumed similar structure. The fulleride $Yb_{2.75}C_{60}$ (Ref. 5) is indeed unusual. Its nonintegral stoichiometry arises from ordered vacancies, and the resulting doubled unit cell of 2008 atoms makes it the largest known superconducting system. Furthermore, there is a preferred rotational ordering of C_{60} pentagonal, not hexagonal, faces towards divalent, not trivalent, Yb cations.

To obtain further information about the charge state of Yb and its local structural and vibrational properties, x-ray absorption and Raman measurements from crystalline and heated $Yb_{2.75}C_{60}$ have been performed. The results reported here are surprizingly rich, yielding insight into the distinctive structure of $Yb_{2.75}C_{60}$ and the general properties and preparative limitations of other intercalated fullerides.

It is useful to summarize the most noteworthy features obtained by x-ray diffraction (XRD).[5] First, the fcc-based subcell of four C_{60} molecules has Yb cations occupying all four octahedral (O) interstitial sites but only seven of the eight tetrahedral (T) sites. The unoccupied site alternates between adjacent T sites in each direction, leading to a unit-cell doubling with eight ordered vacancies. Second, the O-site Yb cations are displaced from the centers of their interstices by ~ 2.4 Å towards the nearest-neighbor (NN) vacancy, effectively reducing the first NN coordination of C_{60} anions around the O-site cations from six to three. There are also small off-center displacements (~ 0.3 Å) of the T-site cations. Third, all C_{60} anions are rotationally ordered to maximize the number of pentagonal (p) faces oriented towards the NN cations. A schematic picture of one of the subcells is shown in Fig. 1.

The vacancy ordering, cation displacements, and anion rotations each break different crystallographic degeneracies. Thus, in the unit cell there are three types of C_{60} molecules: *(1)* four with two NN vacancies, *(2)* 24 with one vacancy, and *(3)* four with 0 vacancies. There are also four types of Yb cations with respect to a vacancy: *(i)* 24 in T sites that are first NN, *(ii)* 24 in T sites, second NN, *(iii)* eight in T sites, third NN, and *(iv)* 32 in O sites, first NN. Finally, in a given subcell there are three types of C_{60} environments around the Yb cations: (a) three first NN p faces, (b) two first NN p faces, and (c) one first NN p face and one first NN hexagonal (h) face. The different components are labeled in Fig. 1, and the different C_{60} environments are listed in Table I. Note that the 11 Yb cations in a subcell are facing 36 p faces out of a possible 48 [(4 C_{60} molecules) $\times$ (12 p faces per molecule)], i.e., 75%, which is the largest allowed fraction in an fcc structure. Schematic views of three local environments around the cations are shown in Fig. 2. Dotted lines between Yb and first NN C atoms are drawn to indicate that, in addition to interstitial-site displacements, the cations are also not centered with respect to the surrounding p faces.

This structure raises a number of questions. Why are there ordered vacancies? What is the significance, if any, of the rotationally ordered C_{60} p faces? Is there a relationship be-

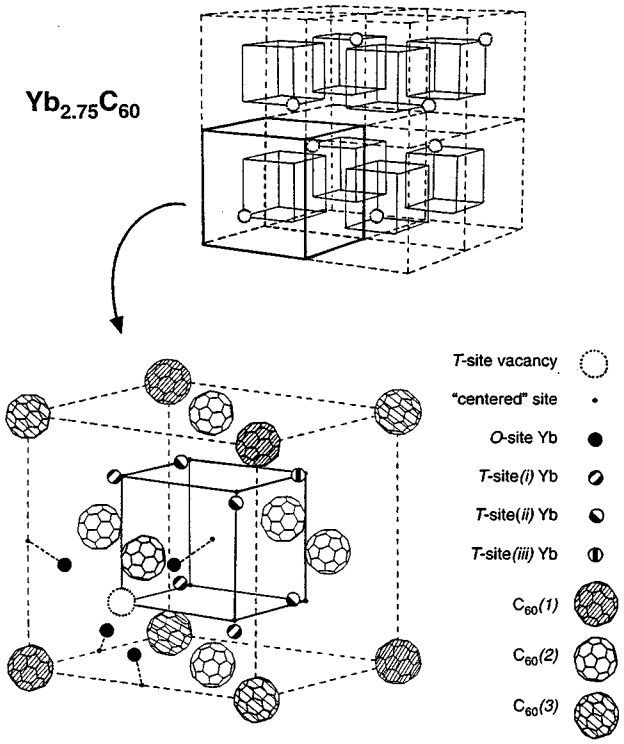

FIG. 1. Schematic structure of $Yb_{2.75}C_{60}$ determined in Ref. 5. Top: In an fcc-based C_{60} subcell, eight of which comprise the full unit cell, the eight tetrahedral (T) interstitial sites that can be occupied by Yb ions are shown connected by thin solid lines. In each subcell a different T site is unoccupied, leading to eight ordered vacancies per unit cell. Bottom: Expanded view of one fcc C_{60} subcell, showing the vacancy, C_{60} anions, and T-site and octahedral (O)-site Yb cations. For clarity, anions and cations are not drawn scaled (approximate real dimensions: fcc sublattice side, 14 Å; C_{60} molecular radius, 3.5 Å; Yb^{2+} ionic radius, 1 Å). O-site cations are displaced ~2.4 Å from their ideal, centered positions in the direction of the vacancy, while T-site cations are displaced in either x, y, or z directions ~0.3 Å (drawn exaggerated). Actual rotational ordering of C_{60} molecules shown here is more apparent in Fig. 2 of Ref. 5. The ordered vacancy leads to three types of C_{60} anions and three types of T-site Yb cations.

tween the p-face ordering and the vacancies and/or the displacements? What can be learned about the limits of fullerene intercalation, e.g., are trivalent metal donors likely or possible? Are there parallels with other organometallic, fulleride, or superconducting compounds that help elucidate the structure of $Yb_{2.75}C_{60}$? The goals of this paper are to address each of these questions using a model developed in the Discussion section, and to stimulate further study of doped fullerene systems.

II. EXPERIMENT

The $Yb_{2.75}C_{60}$ compound, whose stoichiometry has been well established from x-ray diffraction measurements, was prepared as described elsewhere.[5] The extremely air-sensitive fulleride required special handling procedures for transport to and transfer into the ultra-high-vacuum x-ray absorption measurement chamber of the Bell Laboratories X15B beamline[7] at the National Synchrotron Light Source.

TABLE I. Local C_{60} environments surrounding Yb cations.

Yb cation[a]	First NN faces	Second NN faces	Total p faces
T site			
type-(i)			
(1,1)	$2p$	$2p$	4
(1,2)	$2p$	$2p$	4
(1,3)	$1p+1h$	$2p$	3
type-(ii)			
(2,1)	$1p+1h$	$2p$	3
(2,2)	$1p+1h$	$2p$	3
(2,3)	$1p+1h$	$2p$	3
type-(iii)			
(3)	$2p$	$2p$	4
O site			
(4,1)	$3p$	[b]	3
(4,2)	$3p$	[b]	3
(4,3)	$3p$	[b]	3
(4,4)	$3p$	[b]	3
			36

[a]Notation from Ref. 5.
[b]Too distant.

A variety of samples were investigated and found to give reproducible results. The experiments involving *in vacuo* heating of the $Yb_{2.75}C_{60}$ samples resulted in amorphization and powdering of the single-crystal material. This necessitated that, prior to e-beam heating from the back, the crystalline samples be encapsulated in a Ta boat with an x-ray-transparent cover (a 0.1-mm-thick synthetic diamond) to prevent loss of powdered material into the chamber. The thickness of material and method of encapsulation resulted in a nonuniform heating of the material. Fluorescence-yield detection was used to monitor the Yb L_3-edge absorption and to minimize contributions from possible surface contamination (the penetration depth of 7.4-keV Yb $L_3\alpha$ x-ray emission exceeds 30 μm in $Yb_{2.75}C_{60}$ and 0.5 mm in diamond). Measurements from $Yb_{2.75}C_{60}$ samples were performed in a $\sim 1\times10^{-10}$-Torr vacuum and cooled to <60 K to reduce effects of thermal disorder.[8] Absorption data from three reference compounds at 77 K were obtained with total-electron-yield detection in a separate chamber at $\sim 10^{-8}$ Torr. The reference compounds were (1) Yb(η^5-Cp)$_3$ for Yb-C scattering [Cp≡cyclopentadienyl, C_5H_5; $\eta^5\rightarrow$symmetrically five-fold coordinated], (2) Yb(acac)$_3$ for Yb-O scattering [acac≡acetylacetonate, $CH_3COCHCOCH_3$], and (3) evaporated high-purity Yb metal for Yb-Yb scattering. Effects of surface oxygen or moisture contamination, which could be readily observed in intentionally exposed samples, are absent from all data presented here.

For the Raman measurements, the $Yb_{2.75}C_{60}$ powder was placed in a 0.5-mm-diam thin-walled glass ampule and sealed under inert atmosphere. Spectra from room-temperature samples were obtained using 10 mW of Ar-ion laser emission (5145 Å), focused with a cylindrical lens to a line superposed on the axis of the ampule. The ampule image was aligned with the entrance slit of a Spex Triplemate spec-

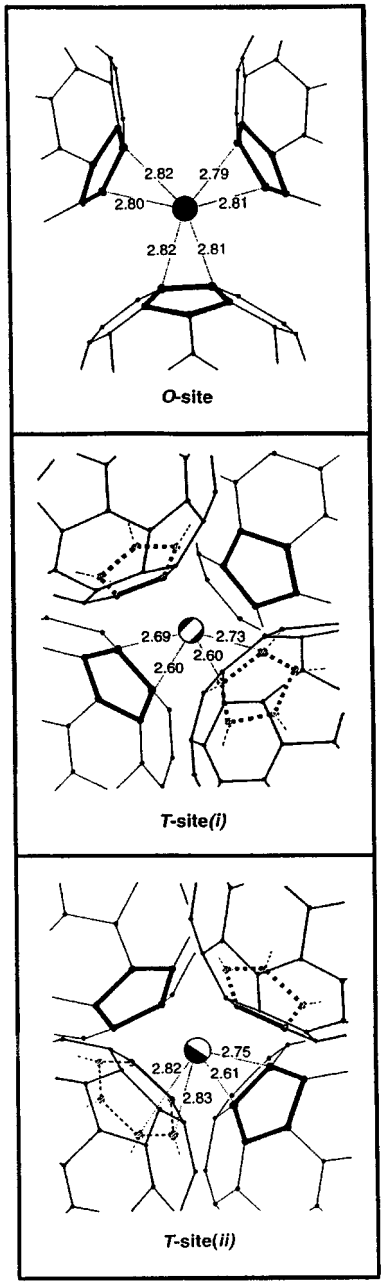

FIG. 2. Local environments around three different Yb cations using coordinates in Ref. 5, (see Fig. 1 and Table I for notation). Top: A ~2.4-Å displacement of *O*-site cations [labeled Yb($4n$) in Ref. 5] leads to three rather than six first nearest-neighbor (NN) C_{60} anions, each with a pentagonal (p) face rotated toward Yb Dotted lines between Yb and NN C atoms (Yb-C distances in Å) indicate that cations are not centered with respect to p faces. Middle: A *T*-site*(i)* cation [labeled Yb(12) in Ref. 5] is surrounded by four anions, two of which are slightly closer due to a ~0.3-Å cation displacement. Each anion is rotated with a p face toward Yb (dotted p faces are behind plane of figure). Bottom: A ~0.3-Å-displaced *T*-site*(ii)* cation [labeled Yb(23) in Ref. 5] is surrounded by four C_{60} anions, two of which are somewhat closer. Icosohedral symmetry of C_{60} is incompatible with fcc packing of $Yb_{2.75}C_{60}$, so all p faces cannot be rotated towards all Yb, i.e., a hexagonal (h) face must be facing a *T*-site*(ii)* cation. *T*-site*(ii)* cations are not centered with respect to either NN p or h faces.

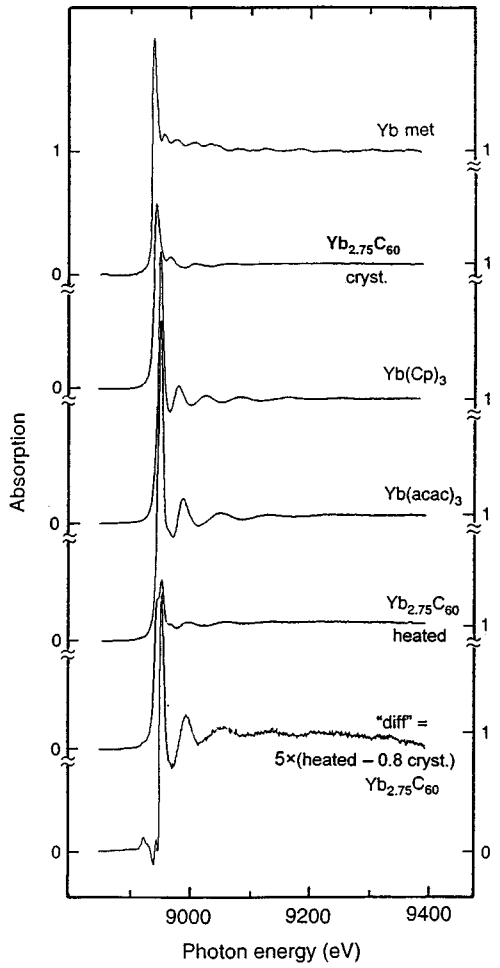

FIG. 3. Raw Yb L_3-edge x-ray absorption data from as-prepared (crystalline) $Yb_{2.75}C_{60}$, heated $Yb_{2.75}C_{60}$, and the three reference compounds Yb metal, $Yb(Cp)_3$ [Cp≡cyclopentadienyl, C_5H_5], and $Yb(acac)_3$ [acac≡acetylacetonate, $CH_3COCHCOCH_3$]. Lower trace labeled ''diff'' represents difference spectrum between heated $Yb_{2.75}C_{60}$ data and 80% of crystalline $Yb_{2.75}C_{60}$ data (see text). All spectra, including ''diff,'' are normalized to unity edge jump.

trometer to optimize collection efficiency. The output of the spectrometer's charge-coupled-device camera was corrected for spectral responses of both the instrument and camera. The incident and scattered radiation were polarized normal to the scattering plane, providing a spectrum which is an average of the diagonal components of the Raman tensor.

III. RESULTS

The top of four spectra in Fig. 3 are raw Yb L_3-edge x-ray absorption data from $Yb_{2.75}C_{60}$ and three reference compounds. All data have been normalized to common edge-jump values at 9.3 keV where the x-ray absorption intensities are structureless (i.e., atomiclike).[8] Features lying between the region just below the edge and about 30 eV above threshold, called the near-edge x-ray absorption fine structure (NEXAFS), contain information about local electronic structure of the absorbing Yb atom. An expanded scale of this near-edge region is shown in Fig. 4. The edge position reflects the Yb $2p_{3/2}$ binding energy, while its shape reflects

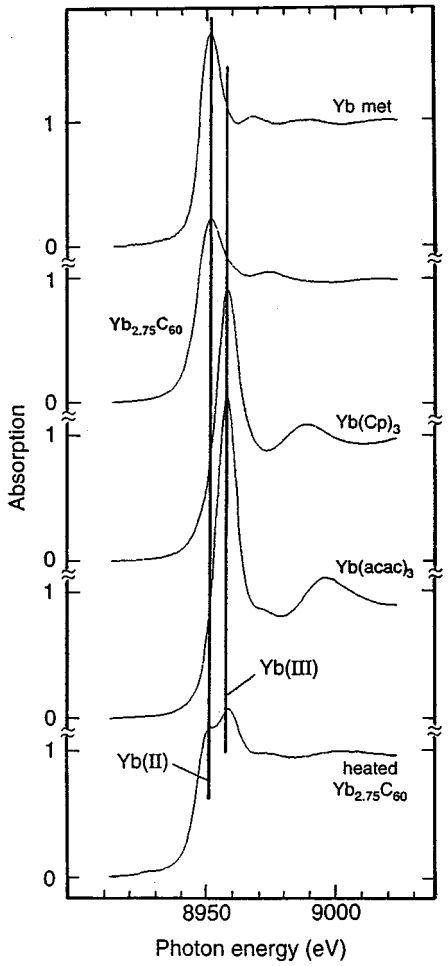

FIG. 4. Raw Yb L_3-edge x-ray absorption data in Fig. 3, expanded in threshold region (see Fig. 3 caption for notation). Vertical lines drawn through near-edge absorption peaks (the so-called ''white lines'') in Yb metal, $Yb(Cp)_3$, and $Yb(acac)_3$ serve as guides to distinguish between Yb(II) and Yb(III) and to identify the Yb(II) state in as-prepared (crystalline) $Yb_{2.75}C_{60}$.

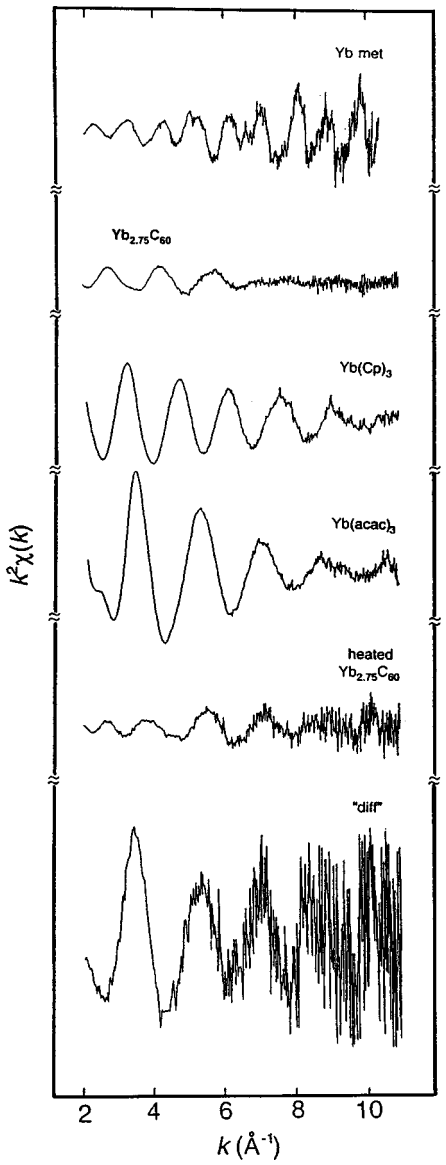

FIG. 5. Edge-jump-normalized EXAFS, $\chi(k)$, weighted by k^2, obtained from Yb L_3-edge data in Fig. 3, after truncating those data above the edge and subtracting a smooth background (see Fig. 3 caption for sample labeling). Differences in EXAFS amplitude and frequency directly reflect different local structures around Yb in $Yb_{2.75}C_{60}$ and the other systems.

the relative energy and localized nature of the lowest unoccupied Yb $5d$-derived state. Both features clearly distinguish the divalent state in Yb metal, i.e., Yb(II)($4f^{14}6s^2$), from the trivalent state in $Yb(Cp)_3$ and $Yb(acac)_3$, i.e., Yb(III)($4f^{13}6s^25d^1$). The NEXAFS measurement from $Yb_{2.75}C_{60}$ makes identification of the Yb(II) charge state—and the absence of Yb(III)—unambiguous.

The region >30 eV above the edge contains the extended x-ray absorption fine structure (EXAFS), $\chi(k)$, which provides local geometric structural information around the Yb cations. For a shell of type-b neighbors, N in number, at a distance R from the absorbing atom a, the usual expressions for $\chi(k)$ and its amplitude function $A_b(k)$ are given by

$$\chi(k)=A_b(k)\sin[2kR+\phi_{ab}(k)], \tag{1}$$

$$A_b(k)\approx N[f_b(\pi,k)/R^2]\exp[-2k^2\sigma^2(k)]\exp[-2R/\lambda(k)], \tag{2}$$

where $\phi_{ab}(k)$ is the phase shift from the absorbing and backscattering atoms, $f_b(\pi,k)$ is the backscattering amplitude for type b atoms, $\exp[-2k^2\sigma(k)^2]$ is a Debye-Waller-like term describing static and thermal disorder with an effective rms deviation $\sigma(k)$, and $\exp[-2R/\lambda(k)]$ is an inelastic loss factor with effective electron mean free path $\lambda(k)$. Following standard analysis procedures[8] for isolating $\chi(k)$ from the structureless atomic background, raw data are truncated above the edge, a smooth background is removed, and the data are converted from photoelectron energy space into photoelectron momentum (k) space, weighted by k^2. The results are displayed in Fig. 5. The oscillatory EXAFS in the top four systems show clear differences in both amplitude and frequency because both $A(k)$ and R are very different. Fourier transforms (FT) of the background-subtracted, k^2-multiplied data from $Yb_{2.75}C_{60}$ and the three model compounds are shown in Fig. 6. The most prominent FT peaks (uncorrected for phase shifts) from Yb metal, $Yb(Cp)_3$ and

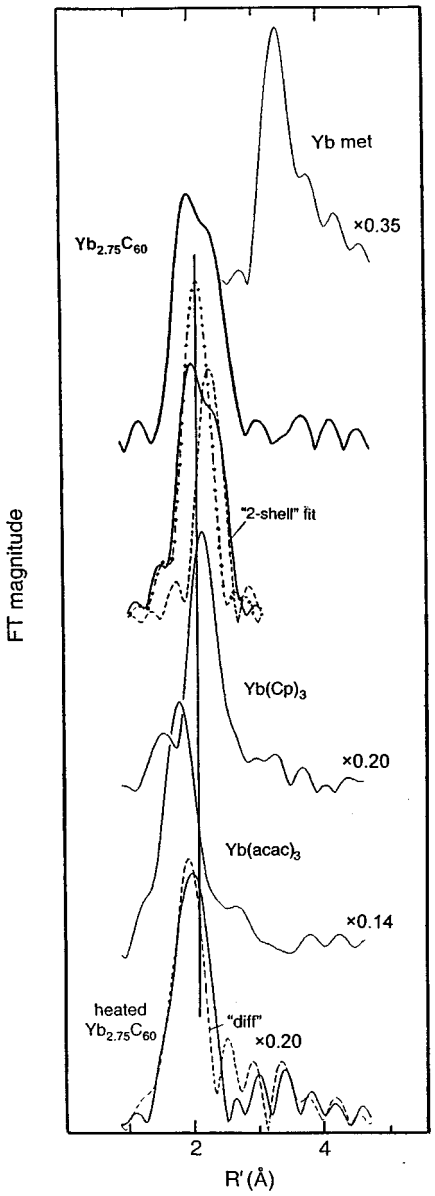

FIG. 6. Fourier transforms (FT) of EXAFS data from Fig. 5 (see Fig. 3 caption for sample labeling). Note different scale factors for FT magnitudes. Dominant FT peak positions in Yb metal, $Yb(Cp)_3$, and $Yb(acac)_3$ correspond to first-neighbor Yb-Yb, Yb-C, and Yb-O distances, respectively (FT peak positions are uncorrected for phase shifts, explaining the R' notation). Comparatively broader and weaker two-peaked FT structure for $Yb_{2.75}C_{60}$ is shown as a heavy solid line. FT results of least-squares fitting with two shells (see Fig. 7) are indicated below the data by a solid line, with individual shells shown as dot-dashed and dashed lines. Solid vertical line is a guide for comparing the different systems.

$Yb(acac)_3$ correspond, respectively, to first-NN Yb-Yb, Yb-C, and Yb-O distances of $R_1 = 3.88$,[9] 2.64,[10] and 2.27 Å.[11] In contrast with these relatively narrow-peaked FT data, a broader two-peaked structure of considerably lower magnitude (note different scales) is observed for $Yb_{2.75}C_{60}$.

The FT data from $Yb_{2.75}C_{60}$ are further analyzed by placing a window function around the two-peaked structure and then transforming back into k space. The result is shown as a bold solid line in Fig. 7. Assuming only two near-neighbor

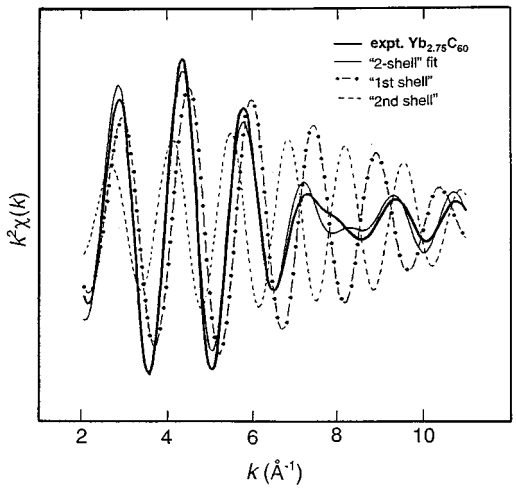

FIG. 7. Result of least-squares fitting the filtered EXAFS data from $Yb_{2.75}C_{60}$ (heavy solid line), obtained by backtransforming the FT data in Fig. 6 over a region of $R' = 1.4$–2.9 Å. The fit, using two ''shells'' and including Debye-Waller-like damping, is indicated by a thin solid line (see text for explanation of quotes). FT results of the fit and of the individual shells are shown in Fig. 6. Yb-C distances determined from the fit are 2.66 ± 0.04 and 2.85 ± 0.04 Å.

shells, a least-squares fit[8] to the filtered data is obtained using $Yb(Cp)_3$ as the model Yb-C system for phase shift and amplitude function information. The result of the ''2-shell'' fit is shown as a thin solid line in Fig. 7 (the quotation marks are explained in Sec. IV B). The individual ''shells'' are also shown as dot-dashed and dashed curves at respective Yb-C distances of 2.66 ± 0.04 and 2.85 ± 0.04 Å and relative intensities of 1.2 ± 0.5.[12] Fourier transforms of the fitted data and of the individual shells are displayed in Fig. 6. Part of the reason for the reduced FT magnitude of the combined shells is seen to be due to the destructive interference of their individual out-of-phase EXAFS at values of $k > 6$ Å. Other reasons for the reduced FT magnitude are discussed in the next section.

Heating the $Yb_{2.75}C_{60}$ sample above 670 °C *in vacuo* and cooling to room temperature results in the next-to-bottom trace in Fig. 1. The NEXAFS of that spectrum is shown in the bottom of Fig. 4. A loss of spectral intensity associated with Yb(II) and a corresponding increase of intensity associated with Yb(III) are apparent. [Complete conversion to the Yb(III) state was not observed, perhaps due to the nonuniform heating of the sample.] To isolate the contribution of Yb(III)-containing material, we used the spectrum from as-grown $Yb_{2.75}C_{60}$ as a model for the residual Yb(II) component and subtracted 80% of its intensity from the total ''heated'' data [such a large amount was needed to remove all Yb(II)-derived signal]. The raw difference spectrum, appropriately renormalized to its edge jump, is the bottom trace in Fig. 3. The corresponding background-subtracted and FT data are given at the bottom of Figs. 5 and 6. Despite the noisier quality of the difference spectra, there is obviously a close resemblance to $Yb(acac)_3$ in both phase and amplitude. While not shown here, only a small amount (about 20%) of the subtracted Yb(II) absorption spectrum is found to correspond to crystalline $Yb_{2.75}C_{60}$; the remainder of that sub-

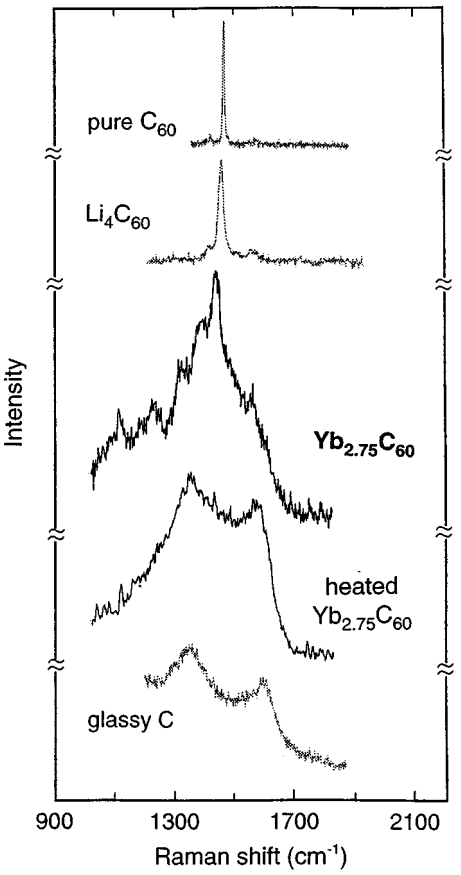

FIG. 8. Raman data from as-grown and heated $Yb_{2.75}C_{60}$ in the region of the C_{60} pentagonal-pinch mode. Both spectra are distinct from one another and are dramatically different from typical data of alkali fulleride compounds, e.g., Li_4C_{60}. Data from heated $Yb_{2.75}C_{60}$ are similar to those from glassy C powder.

tracted spectrum lacks short-range order, i.e., it is amorphous. This fact, coupled with the similarity in phase shift between C and O (in acac) as a near-neighbor scattering atom,[8] indicates that the heated $Yb_{2.75}C_{60}$ sample is a mixture of three components: (1) $\sim 10-20\,\%$ of crystalline, as-grown $Yb_{2.75}C_{60}$, (2) $\sim 60-70\,\%$ of disordered (amorphous) $Yb_{2.75}C_{60}$, and (3) $\sim 20\%$ of a form of Yb carbide with Yb in the trivalent state. Indeed, analysis of the difference data using $Yb(Cp)_3$ as a model gives a Yb-C distance of 2.41 ± 0.04 Å, a value identical to the Yb-C distance in YbC_2,[13] where Yb is mainly in the Yb(III) state.

Supporting evidence for and additional information about these findings are provided by Raman data obtained in the region of the C_{60} pentagonal-pinch mode;[14] see Fig. 8. The as-grown and heated $Yb_{2.75}C_{60}$ samples exhibit strikingly different spectra. Furthermore, both are very different from that of pure C_{60} and from typical data of alkali fulleride compounds, exemplified by the Li_4C_{60} spectrum shown in the top part of the figure. The spectrum of the heated $Yb_{2.75}C_{60}$ sample bears a strong resemblance to that of glassy C powder shown at the bottom of the figure. This result is consistent with the assignment of largely disordered $Yb_{2.75}C_{60}$ in the x-ray absorption spectrum of the heated material.

The crystalline, as-grown $Yb_{2.75}C_{60}$ data exhibit a rich set of overlapping lines, spanning a range of several hundred cm^{-1}, which is far beyond any shift attributable to simple charging of the C_{60} molecule.[15] As seen in Fig. 8, such shifts, typified by the alkali fullerides, are generally only a few tens of cm^{-1}. The crystalline material shows a sharp peak near the shifted pentagonal-pinch mode. If this was, in fact, a remnant of that mode, the size of the shift would indicate a large degree of charging of the C_{60} molecule.[16] The remainder of the spectrum strongly suggests that the molecule is distorted, destroying the degeneracy of the various pinch modes in the symmetric molecule and shifting the other components of the peak by very large amounts. The depolarized spectrum (not shown) is weaker, but shows a structure nearly identical to that of the polarized component displayed in Fig. 8. Indications for distortion of the C_{60} molecular anions are also found in the analysis of the EXAFS data, described below.

IV. DISCUSSION

A. Divalent charge state of Yb cations

Because there are many examples of compounds containing inequivalently charged cations, particularly in the case of rare-earth systems,[17] any meaningful understanding of $Yb_{2.75}C_{60}$ must begin with a knowledge of the Yb charge state(s). Indeed, a photoemission study[18] of thin-film samples of Yb-C_{60} has suggested that the Yb cations are of mixed-valent character, i.e., Yb^{3+} and Yb^{2+} coexist [we shall use formal valence states interchangeably with the notation of formal charge states Yb(III) and Yb(II)]. Another photoemission work of similarly prepared samples suggested that the stoichiometry of the films is Yb_2C_{60}.[19] Previous x-ray diffraction measurements from the bulk Yb-C_{60} samples studied here have established that, in at least the ordered part(s) of these samples from which diffraction is obtained, the stoichiometry is definitively $Yb_{2.75}C_{60}$.[5] However, the degree to which those bulk samples are uniformly ordered (i.e., single crystal), and the actual charge state(s) of the Yb cations in the ordered and possibly disordered other regions, could not be determined using x-ray diffraction. Thus, ordered regions containing either a Yb mixed-valent character, or only Yb^{2+}, or only Yb^{3+}, combined with *disordered* regions containing an identical or different charge-state distribution of Yb could be present and go undetected with x-ray diffraction.

Regardless of the degree of order in the bulk $Yb_{2.75}C_{60}$ material, the formal charge state of Yb obviously has direct implications for the formal charge state of C_{60}. Rewriting $(Yb^{x+})_{2.75}(C_{60}{}^{y-})_1$ in terms of the four C_{60} anions per subcell, i.e., $(Yb^{x+})_{11}(C_{60}{}^{y-})_4$, shows only that $11x=4y$, not what the actual formal values of x and y are, not whether y is integral, and not whether the ions are electronically equivalent. Thus, both cations and anions could be electronically equivalent with y being nonintegral, e.g., $(Yb^{3+})_{11}(C_{60}{}^{8.25-})_4$, or both x and y could be integral with the cations being electronically inequivalent, e.g., $(Yb^{3+})_2(Yb^{2+})_9(C_{60}{}^{6-})_4$. This latter configuration appears to be a particularly likely candidate for two reasons. First, the C_{60} anions would have a formal, conventional six-valence (e.g., K_6C_{60}), and like the anions in almost every single-phase material,[20] they would be equivalently charged. Sec-

ond, about 18% of the Yb cations would be in the 3^+ valence, consistent with the suggestion[18] of a mixed-valent compound.

Our NEXAFS data in Fig. 4 show no measurable evidence for mixed-valent Yb. Instead, they provide direct and conclusive evidence that within the detection limits of the measurement, $<3\%$, Yb in $Yb_{2.75}C_{60}$ is exclusively divalent. These results are independent of the degree to which the various samples studied are homogeneously ordered (a subject discussed in Sec. IV B). They are also in agreement with the prediction,[21] based on Born-Haber cycle calculations, that the divalent state in a Yb fulleride compound is energetically favored over one with Yb in the trivalent state.

As mentioned above, our finding that $x=2$ in $(Yb^{x+})_{11}(C_{60}{}^{y-})_4$ and that the *cations* are electronically equivalent means that the *average* formal charge state for the C_{60} anions must be $5.5-$. It does *not* mean that all of the *anions* are equivalently charged. On the contrary, the fact that y is nonintegral and that the anions are so crystallographically different raises the possibility that the anions could have correspondingly different charge states. To see whether this intriguing situation is plausible, and to learn more about how the charges are distributed on a given C_{60} anion (whatever their absolute value), additional experimental evidence is desirable. Such evidence is discussed below.

B. Local structure around Yb cations: Distorted C_{60} anions

Inspection of Fig. 6 showing the two-peaked FT structure from $Yb_{2.75}C_{60}$, or the analysis of its filtered FT data in Fig. 7 assuming only two Yb-C shells, suggests that the two FT peaks (or two Yb-C shells) simply correspond to the Yb-C distances for the *T*-site and *O*-site cations. This assignment, which actually turns out to be the case, belies a great deal of complexity regarding the local Yb environments. Recall from Figs. 1 and 2 that the *T*- and *O*-site cations are each displaced from the centers of their respective interstitial sites and that they are each configured asymmetrically with respect to the centers of the surrounding C_{60} *p* and *h* faces. The result should therefore be a broad range of many closely spaced Yb-C distances.

Figure 9 displays the number distribution of Yb-C ''shells'' that are expected from a hypothetical EXAFS measurement of $Yb_{2.75}C_{60}$. These shells are calculated from the reported crystal structure,[5] with each bar in the histogram representing the total number of Yb-C distances falling within ± 0.01 Å of values in a grid spaced 0.02 Å apart. The amplitude of each shell has been corrected for damping due to the $1/R^2$ and inelastic-loss terms in Eq. (2) using the reference distance $R_{\rm ref}=2.64$ Å in the compound $Yb(Cp)_3$ (Ref. 10) and using a typical mean free path of $\lambda=10$ Å.[22] No damping correction from the Debye-Waller-like term was made because of its unknown magnitude for the different shells. Finally, all amplitudes have been normalized with respect to the 11 Yb atoms in the $Yb_{11}(C_{60})_4$ subcell. As an illustrative example, the seven *T*-site cations in the subcell have eight Yb-C distances in a shell calculated to lie 2.60–2.62 Å, which is represented by a bar centered at 2.61 Å with amplitude $(8/11)\times(2.64/2.61)^2\times\exp[-2(2.61-2.64)/10]=0.75$. As expected from the above discussion (see Table I and Fig. 9), the distribution of Yb-C distances for the three types of inequivalent *T*-site cations is very rich. The distribution for the *O*-site cations is more simple because all four of these cations are crystallographically equivalent and because the next group of higher-lying C atoms are considerably more distant ($\gtrsim 4$ Å).

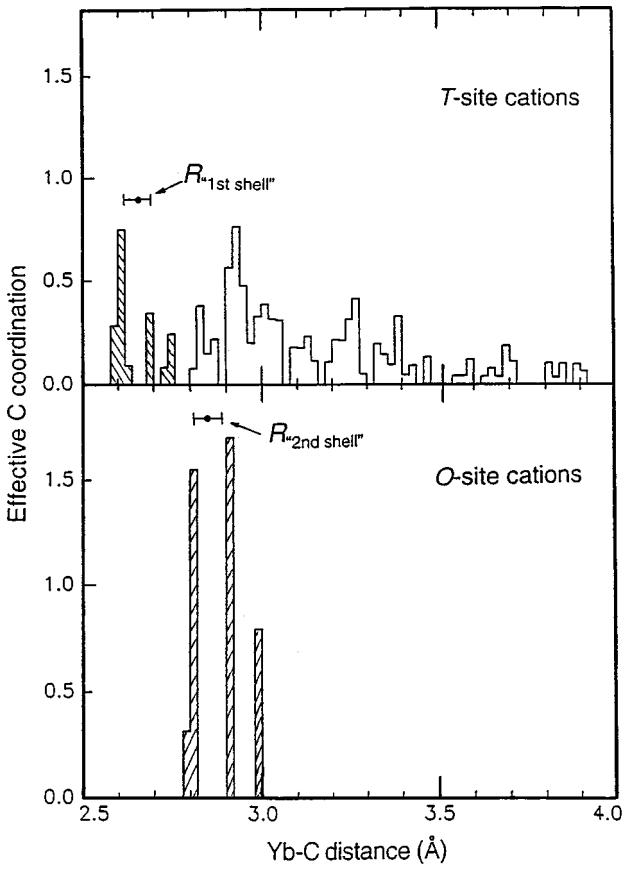

FIG. 9. Histogram of Yb-C shells expected from a hypothetical EXAFS measurement of $Yb_{2.75}C_{60}$. The position of each shell for the tetrahedral (*T*) and octahedral (*O*) Yb cations represents the total number of Yb-C distances, based on the crystal structure from Ref. 5, which fall within ± 0.01 Å of values in a grid spaced 0.02 Å apart. The normalized and corrected amplitude of each shell (see text) represents the effective coordination of C atoms around the *T*- and *O*-site cations (Debye-Waller-like damping is not included). Yb-C values determined from the ''2-shell'' least-squares fit in Fig. 5 are indicated by $R_{\rm 1st\ shell}$ and $R_{\rm 2nd\ shell}$, respectively. A given *R* value corresponds not to a single Yb-C shell but to the average position of a *group* of Yb-C shells, indicated by hatched lines (also see Fig. 10).

Simulated Yb EXAFS data should, in principle, include contributions from *all* the calculated, appropriately damped C shells surrounding both the *T*- and *O*-site Yb cations. Such simulated data in *k* and *R* space are shown in the top of Fig. 10 as a thin solid line, and are compared with experimental data (thick solid line). The obvious disagreement with experiment in phase and amplitude arises largely from the *T*-site shells at Yb-C distances greater than 2.8 Å, and cannot be significantly reduced by including physically reasonable corrections for Debye-Waller-like damping. If, however, we exclude altogether the contributions from these higher-distance *T*-site shells, i.e., truncate *T*-site Yb-C distances greater than 2.8 Å, we obtain the simulated data shown in the

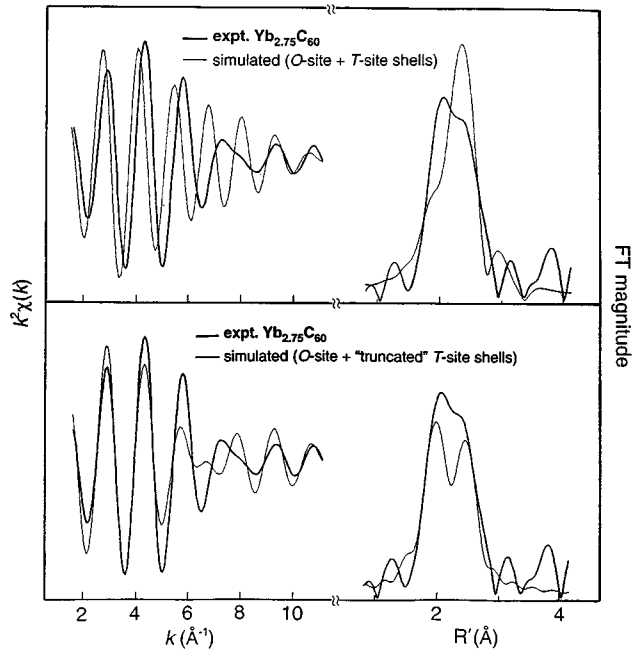

FIG. 10. Comparison of $Yb_{2.75}C_{60}$ filtered and Fourier-transformed experimental EXAFS data with two data simulations, each without Debye-Waller-like damping. Top: Simulation includes all shells of C atoms, calculated in Fig. 9, which surround both the *T*- and *O*-site Yb cations. Disagreement with experimental data in phase (left) and amplitude (right) is apparent, and not greatly improved by including Debye-Waller corrections. Bottom: Simulation includes only those shells of C atoms shown hatched in Fig. 10. Disagreement with experimental data is much smaller and limited mainly to absolute amplitudes. Including Debye-Waller corrections leads to a simulation essentially identical to the ''2-shell'' least-squares fit shown in Figs. 6 and 7.

bottom of Fig. 10. The disagreement with experiment is now much smaller and limited mainly to the absolute amplitudes of the two dominant groups of shells. By including reasonable corrections for Debye-Waller-like damping in these two groups, the simulated data and its parameters become almost indistinguishable from those of the 2-shell least-squares fit shown in Figs. 6 and 7 (explaining why such simulations are not included in Fig. 10). Exploring this trend further by using other selected subsets of shells, e.g., only the first shell for each of the *T*- and *O*-site cations, gives much poorer fits (the need for including the third shell for each of the *T*- and *O*-site cations, however, is less clear).

Two conclusions can be drawn from these results. First, the observed 2-shell structures in Figs. 6 and 7 do indeed correspond to the *T*- and *O*-site cations, but not in an obvious way. That is, the Yb-C distances determined from the 2-shell least-squares fit—denoted in Fig. 9 by $R_{1\text{st shell}}$ and $R_{2\text{nd shell}}$—represent not individual Yb-C shell distances but rather *averaged* values of *groups* of Yb-C shells, one for the *T*-site cations with distances ranging between ~ 2.6 and < 2.8 Å and the other for the *O*-site cations with distances ranging between ~ 2.8 and $\lesssim 3.0$ Å; these groups are indicated by hatching in Fig. 9. This explains why we have used the quoted notation ''2-shell'' fit, ''1st shell'', and ''2nd shell'' in Figs. 6, 7, and 10. [As an aside, the comparatively short Yb-C value of 2.61 Å between the group of first NN C atoms and the *T*-site Yb cations, which are positioned off-center with respect to the *p* or *h* faces (see Fig. 2), might suggest some degree of covalent character in the Yb-C ''bond''. However, similarly off-centered configurations and short Yb-C distances involving Yb^{3+} ions are found in other rare-earth compounds where large charge transfer occurs.[23,24] Inferences about covalency based solely on somewhat shorter, directional ''bonds'' are therefore questionable.]

Second, there is information in the relative EXAFS intensity found for the *T*- and *O*-site group of shells, 1.2 ± 0.5. Although this ratio value is less well established than the corresponding average distance values,[12] the calculated *absolute* intensities of the *combined* *T*- and *O*-site cation groups (which are less strongly correlated to these factors) agree reasonably well with experiment even ignoring any Debye-Waller corrections (see bottom half of Fig. 10) and agree very well with experiment once these corrections are included (see Figs. 6 and 7). Since EXAFS measurements are only sensitive to coherent, short-range order,[8] this agreement demonstrates that the samples studied are quite homogeneous, a point of uncertainty mentioned in Sec. IV A. Furthermore, it means that the small absolute amplitude of the observed EXAFS in $Yb_{2.75}C_{60}$ is due not to the presence of significant regions of disordered material but to the destructive interference of the two dominant *O*- and *T*-site groups of shells. The reason that the effective C coordinations in these groups are themselves so small is that only a limited subset of Yb-C distances is sampled.

What does this result mean? Specifically, what is the significance of the fact that the Yb-C shells for the *O*-site cations at distances $\sim 2.8-3.0$ Å are observed, but the Yb-C shells for the *T*-site cations at comparable distances of less than 2.8 Å are not? The absence of overall disorder within the sample, or (equivalently) the strong degree of order localized around all the individual Yb cations, has been well established in the EXAFS data. Therefore, the nonobservation of certain Yb-C shells in the EXAFS data indicates the presence of some kind of selective disordering for only those C atoms at distances greater than the two (or three) most immediate near-neighbor groups of shells surrounding the *T*-site cations. Although such unusual conditions appear to be inexplicable, supporting evidence for them has already been presented in different but similarly unusual data.

The Raman spectrum from the as-grown $Yb_{2.75}C_{60}$ material in Fig. 8 is remarkably different from that of any other typical metal-doped fulleride. In the spectral range $1200-1600\ \text{cm}^{-1}$, an anomalously broad distribution of vibrational structures with a number of discrete modes is observed. The complexity of the $Yb_{2.75}C_{60}$ system clearly precludes any reliable attempt to identify these various components, because they could result from the splitting of the pentagonal-pinch mode degeneracy, the activation of other previously silent modes, or a combination of both. Nevertheless, the important point here is that such Raman data indicate the C_{60} molecules in $Yb_{2.75}C_{60}$—while still retaining some degree of localized order (hence the discrete structures)—have a substantially lowered symmetry. Simply put, the C_{60} molecules are distorted. This should be compared with the results of the EXAFS data, which show that the C atoms of C_{60}—while strongly ordered in the environment immediately surrounding Yb—are disordered with re-

spect to the *T*-site cations when the C atoms are at slightly more distant positions. From this comparison of independent results we conclude that the selective EXAFS disordering of all but the most localized C shells around Yb is traceable to the distortion of the C_{60} anions.[25] The question now is: Why are the C_{60} anions distorted?

C. Model of $Yb_{2.75}C_{60}$: Role of C_{60} pentagonal faces and of divalent cations

We have identified a distortion of C_{60} anions in $Yb_{2.75}C_{60}$ that is associated with those C atoms not immediately localized around the *T*-site Yb cations. A large departure from the essentially spherical shape of C_{60} must be related to a local, anisotropic interaction with the Yb cations, and therefore more generally with an anisotropic distribution of C_{60} charge. Such a concept is applicable to most fullerene complexes in which the coordinated electron-donating species is covalently bonded,[26,27] but it seems inappropriate for intercalated fulleride compounds in which electron transfer is typically viewed as nearly complete, i.e., ionic.[28] In exploring the underlying reasons for this distortion in $Yb_{2.75}C_{60}$, therefore, it is useful to first consider three, more general questions: (1) Why is C_{60} electronegative? (2) How does C_{60} interact with different types of electron-donating species? (3) Where does the charge that is donated to C_{60} primarily reside? Discussion of these general topics, which are each related to the special role played by the C_{60} *p* faces, will be helpful in providing not only an understanding of the C_{60} distortion but a deeper insight into the anomalous crystallographic features of $Yb_{2.75}C_{60}$. It will also provide the basis for understanding the novel partitioning of donated charge among the different types of C_{60} anions discussed in the next section.

There are two, generically different, but (we will argue) related pictures for describing how C_{60} interacts with electron-donating species. The first is a local picture involving one of the six nonoverlapping and curved (i.e., strained) pyracylene units octahedrally arranged on C_{60}.[26,31] As outlined in Fig. 11, a single unit consists of two *h* faces and two *p* faces,[33] the latter being bridged by a strained and particularly reactive C=C bond.[26,27,31,33] The process of donating one (or two) electron(s) into a pyracylene unit is driven by the electron affinity of the *p* face(s) to form a ''cyclopentadienyl-like'' radical, and by the associated reduction in strain within the negatively charged pentagonal ring(s) upon delocalizing the donated charge (i.e., introducing aromaticity).[34,35] A single pyracylene unit of a C_{60} molecule can, in principle, accept one (or two) electron(s) from a single, strongly nucleophilic (electron-donating) species $\mathscr{N}$, e.g., an alkali-metal atom, leading towards saturation of the C=C bond and redistribution of the donated charge into the pentagonal face(s), as schematically shown in Fig. 11. A less electropositive nucleophile, e.g., an organometallic ligand, can also donate charge to the pyracylene unit, but does so by forming bonds directly with the C atoms comprising the reactive bridging C-C site, i.e., $\mathscr{N}-(\eta^2-C_{60})$.[26,27,31] This description of strongly ionic or covalent donation of charge to fullerenes is clearly a local one, where C_{60} is envisioned not as a globally reactive molecule but instead as a source of isolated reaction sites that are centered at the strained, reactive C=C bonds and the strained, electronegative *p* face(s) of the pyracylene units.

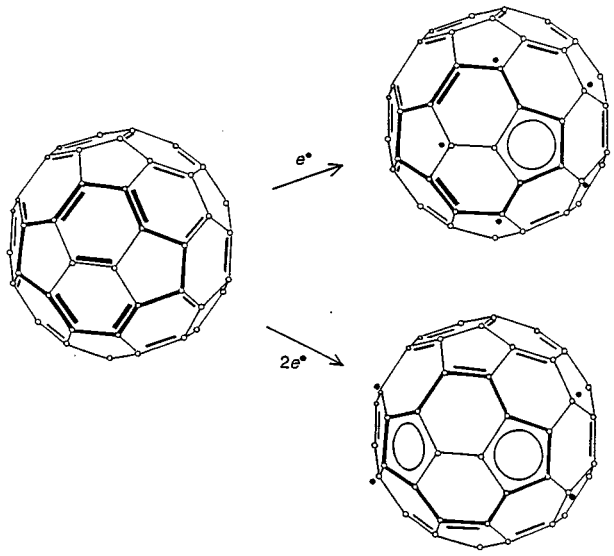

FIG. 11. Schematic, local representation of charge transfer in C_{60} (adapted from Refs. 27 and 32). Left: In neutral C_{60}, one of six strained pyracylene units (outlined in bold lines) consisting of two curved pentagonal (*p*) faces and two curved hexagonal (*h*) faces. Right: The greater electron affinity of the *p* faces drives the pyracylene unit to accept one or two electrons, a process which saturates the reactive C=C bond connecting the two *p* faces, relieves molecular strain, and leads to a delocalization of charge (aromaticity) within the rings (the resulting unpaired electrons are only schematic intermediary representations). This local picture depicts the more electronegative *p* faces of C_{60} as being the primary regions where donated charge resides.

By contrast, a band structure picture of how C_{60} accepts charge considers all the molecular orbitals from all the C atoms.[33,36] The lowest unoccupied molecular orbital (LUMO) of C_{60}, t_{1u}, has octahedral symmetry and can accept six electrons, while the next lowest molecular orbital (LUMO+1), t_{1g}, has the same symmetry and the same filling capacity. Although not usually discussed in these terms, the local picture above makes clear that the LUMO and (LUMO+1) states are related to the very same unfilled orbitals associated with the *p* faces in the six pyracylene units. These six units comprise all 12 *p* faces of the C_{60} molecule, have the same octahedral symmetry as the t_{1u} and t_{1g} states, and accept the same maximum total of 12 electrons as those states. In the case of nearly complete charge transfer, e.g., intercalated alkali fullerides, the first six electrons fill the t_{1u}-derived (LUMO) states that are distributed among the *p* faces in each of the six pyracylene units, while the next six electrons fill the t_{1g}-derived (LUMO+1) states that are also distributed among the *p* faces. This filling sequence promotes a more uniform distribution of charge over the C_{60} molecule, and for a total transfer of up to six electrons avoids forming strained double bonds[31–33] in the normally single-bonded *p* faces (see Fig. 11); the energy barrier to forming these strained double bonds is related to the energy gap between the t_{1u} and t_{1g} states.[36] Calculated charge densities of

t_{1u}-derived states for C_{60}^{6-} ions in K_6C_{60} (Ref. 37) fully support the picture of donated charge residing predominantly within the *p* faces of C_{60}.

These two descriptions of charge transfer to C_{60} provide a useful framework for contrasting how the distribution of donated charge on C_{60} affects its shape. For example, in the complex $[(C_6H_5)_3P]_2Pt\text{-}(\eta^2\text{-}C_{60})$ (Ref. 27) the nominally divalent Pt atom of the nucleophilic species $[(C_6H_5)_3P]_2Pt$ forms covalent bridging bonds with both C atoms of the reactive C=C bond in the pyracylene unit. The formation of the two Pt-C bonds leads to a saturation, and thus lengthening of the C=C bond, as well as a lengthening of the four C-C bonds between the first- and second-neighbor C atoms to Pt; the other single and double bonds in the rest of the C_{60} molecule, however, remain essentially unchanged.[27,38,39] Because the distribution of additional charge on C_{60} is highly localized around only those C atoms close to Pt, the shape of the C_{60} molecule is distorted.

Such a situation should be compared with the intercalated alkali fullerides, A_nC_{60}. Here, the effect of transferring charge from the monovalent alkali-metal atoms to C_{60} is to shorten all of the C-C bonds and to lengthen all of the C=C bonds.[30,40] The alkali fullerides are strongly ionic,[29,41] and the distribution of cations surrounding C_{60} is completely isotropic. There is, therefore, little reason to expect anything but a uniform distribution of transferred charge on the C_{60} anions. That is, the transferred charge is equally distributed among the *p* faces in all six of the pyracylene units, having little effect on the essentially spherical shape of the C_{60} anion.[28]

The above description of an anisotropically distributed donated charge leading to a distortion of C_{60} in systems where the divalent-metal–C_{60} bond is strongly covalent (and, conversely, a more uniformly distributed charge leading to little or no C_{60} distortion when the monovalent-metal–C_{60} ''bond'' is strongly ionic[28]) suggests that the observed distortion of C_{60} in $Yb_{2.75}C_{60}$ is simply due to a strongly covalent Yb-C interaction. Such reasoning, however, can be misleading. It is true that the nature of the Yb-C_{60} ''bond'' in $Yb_{2.75}C_{60}$ should lie somewhere between that in the extreme covalent and ionic examples cited above, and so at least some degree of covalent bonding might be expected between Yb and C_{60}. Indeed, such partial covalent character is calculated, e.g., in the related system Ca_5C_{60} (Ref. 42) (the alkaline-earth Ca^{2+} cation might appear to be very different from that of Yb^{2+}, but its size and organometallic chemistry are actually very similar[43]). It is also true that the apparent directionality of the *T*-site Yb cations towards one or two NN C atoms[5] in the surrounding *p* (or *h*) faces, along with the corresponding Yb-C NN distances being somewhat shorter than those in typically ionic Yb-C materials,[24] are consistent with some covalent Yb-C character in $Yb_{2.75}C_{60}$. However, as noted in the preceding section, such structural features have been observed in other rare-earth compounds that are more consistently described by ionic bonding.[23,24] Therefore, while partial covalency undoubtedly exists in $Yb_{2.75}C_{60}$, it cannot be assumed to be strong.

If a strongly covalent interaction between Yb and C_{60} is not the principal source of the observed distortion of the C_{60} anions, then what is? We argue here that it is the strong and localized electrostatic interaction originating from the Yb cations being divalent and the electronegative C_{60} *p* faces being the primary regions in which the donated charge resides. For a given cation size and separation (and assuming, for simplicity, complete charge transfer), the Ewald interaction between the negatively charged *p* faces of the doped C_{60} anions[34] and the surrounding cations is *four times larger* when the cations are divalent rather than monovalent. Any distortions calculated for alkali-doped fullerides,[29,30] therefore, will be that much smaller than those for fullerides intercalated with divalent cations. (An additional factor for the observed anion distortions, namely, the spatial anisotropy of the surrounding Yb cations, is mentioned in the next section.)

Apart from the distortion of the C_{60} anions, there are two other related crystallographic features which are essentially Coulombic in nature and which further distinguish $Yb_{2.75}C_{60}$ from all of the monovalent alkali fullerides. The first is that the C_{60} *p* faces, not the *h* faces, are preferentially oriented towards the *T*- and *O*-site cations in $Yb_{2.75}C_{60}$ [recall that there is no strong preference for the *p* faces in the fcc fulleride structures A_3C_{60} and Na_2AC_{60} (A=K, Rb, or Cs) (Ref. 41)]. This difference is again traceable to the greater electrostatic attraction for the divalent cations. The rotational preference of the C_{60} *h* faces along the $\langle 111\rangle$ directions in the fcc alkali fullerides is due to the fact that such an orientation accommodates all eight of the *T*-site alkali cations,[44] i.e., geometric factors, such as optimized packing of the *T*-site ions, are more important than electrostatic effects.

The second noteworthy feature of $Yb_{2.75}C_{60}$ is the ordered *T*-site vacancies. To see how these also find their origin from a Coulombic attraction between divalent Yb and electron-rich C_{60} *p* faces,[34] consider the fullerides Ba_3C_{60}, K_3C_{60}, and $Yb_{2.75}C_{60}$. The C_{60} *p* faces in Ba_3C_{60} are, as in $Yb_{2.75}C_{60}$, oriented towards the divalent cations.[45] The size of the Ba^{2+} cations are the same as K^+, but unlike the fcc structure of K_3C_{60}, that of Ba_3C_{60} is bcc (the A15 phase). Conventional electrostatics alone cannot account for the difference between fcc versus bcc packing, as evidenced by the very similar Madelung energy per C_{60} calculated for the A15 phase of $(Ba^{2+})_3C_{60}^{6-}$ and a hypothetical fcc phase of $(Ba^{2+})_3C_{60}^{6-}$.[46] A bcc preference is, however, suggested[45] by considering the energy gained when Ba^{2+} cations are oriented towards the C_{60} *p* faces and placed in the *T* sites of a bcc lattice, the symmetry of which is fully compatible with such a configuration.

Since a bcc lattice can accommodate all C_{60} *p* faces being oriented towards eight *T*-site cations while an fcc lattice cannot, why then is $Yb_{2.75}C_{60}$ based on fcc packing? The reason, we believe, lies with the fact that the Yb^{2+} ionic radius (1.02 Å) is too small for the tetrahedral hole in a bcc-packed C_{60} lattice (1.3–1.4 Å).[45] While interactions with the C_{60} *p* faces would be improved by displacing the *T*-site cations towards the *p* faces of two NN anions in a bcc lattice, a more energetically favorable solution is adopted instead, which is to keep the fcc-packed C_{60} lattice (with its smaller, 1.1-Å tetrahedral hole and accordingly smaller *T*-cation displacements) and then introduce ordered *T*-site vacancies. The removal of one *T*-site Yb per subcell serves the critical function of creating sufficient room for very large displacements of the four

O-site cations towards that vacancy (see Fig. 1). This, in turn, facilitates additional Coulombic interactions between the now-much-closer *O*-site cations and the C_{60} *p* faces (see Fig. 2). We believe it is these additional interactions—brought about by the vacancies—that tilt the balance towards favoring fcc packing.

Summarizing this section, we have argued that the distorted shape of the C_{60} anions and the distinctive crystallographic features observed in $Yb_{2.75}C_{60}$, i.e., the C_{60} *p*-face ordering, the cation displacements, and the *T*-site vacancies, are each traceable to the strong, local interactions between the divalent Yb cations and the inhomogeneously distributed donated charge residing largely in the *p* faces of the C_{60} anions. More theoretical study of these ideas is anticipated.[47]

D. Model of $Yb_{2.75}C_{60}$: Partitioning of donated charge on C_{60} anions

In the spirit of our discussion in Sec. IV C, the general process of charge transfer from a nucleophilic species to a C_{60} molecule can be described within either an extended or local picture. An extended picture of an intercalated alkali fulleride, for example, starts with the known positions of the atoms in the fulleride and applies a first-principles band structure calculation and a state-population analysis to determine how the charge is apportioned. Such an approach has been applied to the case of K_6C_{60}, for example, showing there is almost complete transfer of six e^- from the 6 K atoms to each C_{60} molecule.[30] This calculated ionic character for K_6C_{60} simply means that the charge on the C_{60} anions is essentially the same as what the formally assigned value would be, namely, $6-$. A local picture giving this same result starts with the individual K and C_{60} ions in the bcc lattice and assumes that each monovalent K atom in a *T* site formally donates $\frac{1}{4}\,e^-$ to each of its four NN C_{60} molecules. Since there are 24 such *T*-site K atoms surrounding a given C_{60} molecule, a total of six electrons are transferred.

This local partitioning of formal charge can be extended to other alkali- and alkaline-earth intercalated fullerides. The first eight entries in Table II list selected known fulleride compounds[44,45,48–53] and the formal charge states of the corresponding C_{60} anions ranging from $1-$ to $12-$. In the fcc structure of K_3C_{60}, for example, a C_{60} anion of $3-$ formal charge is surrounded by eight *T*-site K^+ cations and six *O*-site K^+ cations. Each of these cations formally contributes $\frac{1}{4}\,e^-$ and $\frac{1}{6}\,e^-$ to each of its four and six NN C_{60} ions, respectively, giving a net transfer of three e^- $[8(\frac{1}{4}\,e^-)+6(\frac{1}{6}\,e^-)]$ to any given C_{60} anion. If the cation in this particular system were divalent, e.g., Ba_3C_{60} in a hypothetical fcc structure (see Table II), then the *T*- and *O*-site Ba^{2+} cations would transfer six e^- $[8(\frac{1}{2}\,e^-)+6(\frac{1}{3}\,e^-)]$ to any given C_{60} anion. Note that this bookkeeping of formally donated charge is based only on the cation valence, its NN coordination, and the assumption that the total amount of formal charge transferred from a particular cation is independent of its crystallographic site.

In view of the simple structure and stoichiometry of these fullerides, the above partitioning of cation formal charges would seem to be cumbersome and unnecessary. Its utility only becomes apparent when considering $Yb_{2.75}C_{60}$, whose structure and stoichiometry are anything but simple. The *T*-site Yb^{2+} cations formally contribute the same $\frac{1}{2}\,e^-$ to each of its four NN C_{60} anions, as does the Ba^{2+} cations in Ba_3C_{60} (bcc), Ba_6C_{60} (bcc), and Ba_3C_{60} (hypothetical fcc). The *O*-site Yb^{2+} cations in $Yb_{2.75}C_{60}$, however, because of their 2.4-Å displacements towards the *T*-site vacancy,[5] have effectively three rather than six NN C_{60} anions and thus donate twice as much formal charge, i.e., $\frac{2}{3}\,e^-$. Even more different is that, unlike all other known intercalated fullerides with integral anion charge states, the C_{60} anions have three very different NN cation environments. Specifically, [see Fig. 2(b) of Ref. 5], type-*(1)* anions with two vacancies have 12 NN cations (six *O*-site and six *T*-site), type-*(2)* anions with one vacancy have ten NN cations (three *O*-site and seven *T*-site), and type-*(3)* anions with 0 vacancies have eight NN cations (all *T*-site). Thus, the amount of charge donated to type-*(2)* anions on the faces of the $(C_{60})_4$ sublattice is $5.5\,e^-$ $[7(\frac{1}{2}\,e^-)+3(\frac{2}{3}\,e^-)]$, which is just the average formal C_{60} charge state in $Yb_{2.75}C_{60}$. Type-*(1)* and type-*(3)* C_{60} anions in the corners of the subcell, however, have charges of $7\,e^-$ $[6(\frac{1}{2}\,e^-)+6(\frac{2}{3}\,e^-)]$ and $4\,e^-$ $[8(\frac{1}{2}\,e^-)]$, which are quite different from $5.5\,e^-$ and even more different from one another. The resulting subcell stoichiometry is thus $(Yb^{2+})_{11}(C_{60}^{5.5-})_3(C_{60}^{4-})_{0.5}(C_{60}^{7-})_{0.5}$. A full account of the bookkeeping is given in Table III.

TABLE II. Partitioning of formal charge on M_xC_{60}.

M_xC_{60}	phase	*T*-site *M* charge per C_{60}	*O*-site *M* charge per C_{60}	C_{60} charge (total)
KC_{60}	fcc[a]		$+\frac{1}{6}$	-1
Na_2C_{60}	fcc[b]	$+\frac{1}{4}$		-2
K_3C_{60}	fcc[c]	$+\frac{1}{4}$	$+\frac{1}{6}$	-3
K_4C_{60}	bcf[d]	$+\frac{1}{4}$		-4
KBa_2C_{60}	fcc[e]	$+\frac{1}{2}$	$+\frac{1}{6}$	-5
K_6C_{60}	bcc[f]	$+\frac{1}{4}$		-6
Ba_3C_{60}	bcc[g]	$+\frac{1}{2}$		-6
Ba_6C_{60}	bcc[h]	$+\frac{1}{2}$		-12
Ba_3C_{60}	fcc[i]	$+\frac{1}{2}$	$+\frac{1}{3}$	-6
$Yb_{2.75}C_{60}$	fcc[j]	$+\frac{1}{2}$	$+\frac{2}{3}$	-5.5

[a]Reference 48.
[b]Reference 49.
[c]Reference 44.
[d]Reference 50.
[e]Reference 51.
[f]Reference 52.
[g]Reference 45.
[h]Reference 53.
[i]Hypothetical.
[j]Reference 5.

The above partitioning of charge cannot be taken literally, of course, for at least two reasons. First, it is based on formal rather than actual charges. In the case of $Yb_{2.75}C_{60}$, this translates into considering how much of the $6s^2$-like charge in Yb(II)$(4f^{14}6s^2)$ is transferred to C_{60}, i.e., how large δ is in $Yb^{(2-\delta)+}$. We have mentioned above that δ is most likely non-negligible because charge transfer from Yb is less complete than from the more electropositive alkali metals, so our partitioning of transferred charge would be more appropriately written as $(Yb^{(2-\delta)+})_{11}(C_{60}^{(2.75)(2-\delta)-})_3(C_{60}^{(2)(2-\delta)-})_{0.5}(C_{60}^{(3.5)(2-\delta)-})_{0.5}$. Second, even assuming there was complete charge transfer in

TABLE III. Formal charge on C_{60} anions based on nearest-neighbor Yb cations.

Type of C_{60} anion	Type of Yb cation	Number of NN C_{60}'s	Formal charge per C_{60}	Formal charge per C_{60}
(1)	*O* site	6	$\frac{2}{3}\ e^-$	$4\ e^-$
	T site *(ii)*	6	$\frac{1}{2}\ e^-$	$3\ e^-$
				$7\ e^-$
(2)	*O* site	3	$\frac{2}{3}\ e^-$	$2\ e^-$
	T site *(i)*	3	$\frac{1}{2}\ e^-$	$1.5\ e^-$
	T site *(ii)*	3	$\frac{1}{2}\ e^-$	$1.5\ e^-$
	T site *(iii)*	1	$\frac{1}{2}\ e^-$	$0.5\ e^-$
				$5.5\ e^-$
(3)	*T* site *(i)*	6	$\frac{1}{2}\ e^-$	$3\ e^-$
	T site *(iii)*	2	$\frac{1}{2}\ e^-$	$1\ e^-$
				$4\ e^-$

$Yb_{2.75}C_{60}$, i.e., $\delta=0$, formal partitioning does not consider how different donated charges would actually be distributed on a given anion, i.e., the local electronic structure of the different anions is ignored. Related to this is the total energy of the system, i.e., the ultimate degree of charge that is actually transferred between the type-*(1)* and type-*(3)* anions. Such effects of local polarization and overall energy minimization might be expressed with a variable γ, e.g., $(Yb^{2+})_{11}(C_{60}^{5.5-})_3(C_{60}^{(4+\gamma)-})_{0.5}(C_{60}^{(7-\gamma)-})_{0.5}$. Determining γ and δ obviously requires calculations beyond the scope of this work, but even with our simplifying neglect of their importance, the essential physical picture remains intact: The three types of crystallographically inequivalent C_{60} anions in $Yb_{2.75}C_{60}$ should be inequivalently charged.

Our proposal for inequivalently charged anions in a single-phase compound is certainly atypical, but it is not without precedent. A very similar situation exists in the class of perovskite-related high-T_c superconductors, arguably among the most well-studied materials within the last decade. The covalent interaction between divalent Cu and O in $YBa_2Cu_3O_7$ (YBCO), for example, is reminiscent of (though stronger than) that between divalent Yb and C in $Yb_{2.75}C_{60}$. More importantly, however, is that YBCO contains three crystallographically inequivalent O anions coordinated either to two Cu atoms in a nearly planar configuration, to two Cu atoms in a straight chain, or to one Cu (planar) and two O (chain) atoms. Denoting the planar, apical, and chain anions by O*(1)*, O*(2)*, and O*(3)*, respectively, allows this cuprate to be written as $YBa_2[Cu(O(1))_2]_2[Cu(O(2))_2O(3)]$. Various calculations[54] have found that the extra anionic charge (in this case a hole rather than an electron) is inequivalently distributed among the different anions, a result recently confirmed with x-ray absorption measurements.[55] Consistent with the above notation, these data indicate a charge distribution of $Y^{3+}(Ba^{2+})_2[(Cu^{2+}(O^{1.90-}))_2]_2[(Cu^{2+}(O^{1.87-}))_2O^{1.66-}]$. The relative charge difference between the O*(1)* and O*(3)* anions of 12% (0.24/2) is substantial, and undoubtedly represents a more realistic range than the upper-limit value of $\sim$55% (3.0/5.5) that was formally assigned between the C_{60}*(1)* and C_{60}*(3)* anions in $Yb_{2.75}C_{60}$ (recall that the effects of incomplete charge transfer, polarization, and energy minimization should each reduce this).

We close this subsection by noting that the unequal amounts of donated charge on the C_{60} anions are expected to affect their shape as well. We argued in Sec. IV C that the strong electrostatic interaction between divalent Yb and the donated charge on C_{60} was responsible for the observed C_{60} distortions. It should now be apparent that the other important contributing factor to the distortions is the asymmetric distribution of the Yb cations. That is, not only is the attraction between Yb^{2+} and the charge residing in the C_{60} *p* faces strong and local, but that interaction is also anisotropic due to the spatial disposition of the Yb cations. We infer, therefore, that the inequivalently charged C_{60} anions in $Yb_{2.75}C_{60}$ should also be inequivalently distorted in shape.

E. Heated $Yb_{2.75}C_{60}$, trivalent Yb, and other fullerides

The x-ray absorption data from $Yb_{2.75}C_{60}$ heated above 670 °C show that $\sim$60–70% of the crystalline sample is converted to a disordered or amorphous material with Yb still in the Yb(II) state, and that another $\sim$20% is converted to a carbide with Yb in the Yb(III) state [the nonuniform sample heating in these measurements may be responsible for incomplete conversion of Yb(II)$\rightarrow$Yb(III)). Raman data from heated $Yb_{2.75}C_{60}$ confirm that a major fraction of the sample resembles a glassy C powder, with any vestige of long-range order among C atoms being completely destroyed. The sequence of disordering the $Yb_{2.75}C_{60}$ crystal structure, dissociating the C_{60}, and promoting divalent Yb into the trivalent state cannot be determined from these data, but it is clear that heating contributes to at least one of these three processes. That heating forms a disordered phase containing Yb(II) is consistent with the narrow range of conditions required to prepare stoichiometrically pure, single-phase $Yb_{2.75}C_{60}$.[5]

The inability to form a stable fulleride with Yb(III) supports theoretical predictions based on simple thermodynamic arguments.[21] The same calculations predict thermodynami-

cally stable intercalated fullerides with Sm and Eu, the only other rare-earth elements known to exist in divalent states as pure metals. The preparation of such compounds has recently been reported,[6,56] although the actual charge states of Sm and Eu remain to be determined. It is worth noting that favorable formation enthalpies have also been calculated for fullerides doped with trivalent La, Ce, Pr, Nd, and Pm,[21] but repeated experimental attempts using these intercalants have thus far been unsuccessful.[57,58] Our proposed arguments stressing the importance of a strong attraction between divalent cations and donated charge within the C_{60} *p* faces may be extended and applied to this problem: The Ewald interaction with a trivalent cation is so large (formally nine times greater than that of a monovalent cation) that it most likely leads to dissociation of C_{60}, explaining why trivalent intercalants in fullerides have been so difficult (if not impossible[59]) to prepare. Further extension of our discussion of rotational *p*-face ordering and of anisotropic charge distribution on C_{60} anions due to such interactions with divalent cations should apply to other alkaline-earth fullerides, even if some of these effects have not yet been observed. For example, at least one reason for the lack of reported *p*-face ordering in the Ca and Sr fullerides[3,58,60,61] is the unavoidable presence of some sample disorder; in one of these fullerides, however, the same stoichiometry (i.e., $Ca_{2.75}C_{60}$) due to ordered vacancies, has been reported.[62] Interestingly, a Raman study of Ca_xC_{60} ($x=3,5$) has been reported[61] which invokes the need for (unspecified) strong interactions between the cations and anions. Finally, there have been recent studies focusing on the existence of small amounts of vacancies ($<10\%$) (Ref. 63) and of *O*-site cation displacements[64,65] from their interstitial centers ($\lesssim 0.7$ Å) even in some alkali-metal fullerides. This has triggered some debate,[65,66] pointing out the need for further study of these additional features in otherwise well-characterized systems, features which turn out to be the cornerstones for understanding the structure of $Yb_{2.75}C_{60}$.

V. CONCLUSIONS

X-ray diffraction from $Yb_{2.75}C_{60}$ has revealed several distinctive structural elements,[5] the most significant of which are the ordered *T*-site vacancies because they make all components in the unit cell crystallographically inequivalent. This may not seem at first to be particularly unusual, considering that any fully intercalated fcc fulleride, e.g., K_3C_{60}, contains both *T*- and *O*-site cations, and by definition these are crystallographically inequivalent. A similar statement applies to the C_{60} anions in mixed-cation systems, e.g., Rb_2CsC_{60}. What distinguishes $Yb_{2.75}C_{60}$ from all other fullerides is that not only are the cations and anions *each* structurally inequivalent, but the degree of their differences is so large. The *O*-site cations are displaced from their interstitial centers by as much as 2.4 Å, and the three types of C_{60} anions are surrounded by 8, 10, or 12 Yb cations. The C_{60} pentagonal faces are also preferentially oriented towards the different cations. The NEXAFS, EXAFS, and Raman results presented here now show that the charge state of all Yb cations is exclusively divalent, thus implying a nonintegral average charge on the C_{60} anions of $5.5-$. Moreover, those C atoms not immediately near Yb cations are sufficiently displaced from their ideal positions to produce measurable distortions of the C_{60} anions.

Based on geometric and electronic properties of known fullerene complexes and fulleride compounds, we have proposed a simple, physically plausible, and unifying model that accounts for all of these structural features in $Yb_{2.75}C_{60}$. Central to the model are the strong, local interactions between the divalent Yb cations and the negative charge donated primarily into the pentagonal faces of the C_{60} anions. The model predicts that the donated charge on a given anion should be anisotropically distributed, and that the total amount of donated charge among the structurally inequivalent anions in the unit cell should also be anisotropically partitioned. This unequal charge distribution is found for O anions in high-T_c superconductors like $YBa_2Cu_3O_7$, but it is unprecedented for C_{60} anions. Some or all of the other distinguishing features observed in $Yb_{2.75}C_{60}$, e.g., vacancies, displacements, and *p*-face ordering, are expected in other energetically stable fullerides intercalated with divalent metals, and may even be important in some alkali-metal fullerides.

ACKNOWLEDGMENTS

The authors thank R. C. Haddon, M. A. Marcus, K. M. Rabe, K. Rhagavachari, and M. Steigerwald for helpful discussions, and E. E. Chaban for skillful technical assistance. Financial support for E.Ö. from the Scientific and Technical Research Council of Turkey through NATO, and for S.S. from the Alexander von Humboldt Foundation, is gratefully acknowledged. The x-ray absorption measurements were performed at the National Synchrotron Light Source, Brookhaven National Laboratory, which is supported by the Department of Energy, Division of Materials Science and Division of Chemical Sciences.

*Present address: Physics Department, Hacettepe University, Ankara 06532, Turkey.

†Present address: Forschungszentrum Karlsruhe, INFP, D-76021 Karlsruhe, Germany.

‡Present address: AT&T Labs-Research, Florham Park, NJ 07932.

[1] For example, see *Science of Fullerenes and Carbon Nanotubes*, by M. S. Dresselhaus, G. Dresselhaus, and P. C. Eklund (Academic, New York, 1996).

[2] A. F. Hebard, M. J. Rosseinsky, R. C. Haddon, D. W. Murphy, S. H. Glarum, T. M. Palstra, A. P. Ramirez, and A. R. Kortan, Nature (London) **350**, 600 (1991).

[3] A. R. Kortan, N. Kopylov, S. Glarum, E. M. Gyorgy, A. P. Ramirez, R. M. Fleming, F. A. Theil, and R. C. Haddon, Nature (London) **355**, 529 (1992).

[4] Of all alkali and alkaline-earth metals, only Be and Mg have not been successfully intercalated in fullerides.

[5] E. Özdaş, A. R. Kortan, N. Kopylov, A. P. Ramirez, T. Siegrist, K. M. Rabe, H. E. Bair, S. Schuppler, and P. H. Citrin, Nature (London) **375**, 126 (1995).

[6] X. H. Chen and G. Roth, Phys. Rev. B **52**, 15 534 (1995).

[7] A. A. MacDowell, T. Hashizume, and P. H. Citrin, Rev. Sci. Instrum. **60**, 1901 (1989).

[8] P. A. Lee, P. H. Citrin, P. Eisenberger, and B. M. Kincaid, Rev. Mod. Phys. **53**, 769 (1981).

[9] A. H. Daane, D. H. Dennison, and F. H. Spedding, J. Am. Chem. Soc. **75**, 2272 (1953).

[10] S. H. Eggers, J. Kopf, and R. D. Fischer, Acta Crystallogr. Sec. C **43**, 2288 (1987).

[11] J. A. Cunningham, D. E. Sands, W. F. Wagner, and M. F. Richardson, Inorg. Chem. **8**, 22 (1969).

[12] The relative amplitude has a large uncertainty because of strong correlation with the Debye-Waller-like damping factors of the two shells. The corresponding shell distances are less correlated, but conservative uncertainties are also quoted.

[13] M. Atoji and R. H. Flowers, J. Chem. Phys. **52**, 6430 (1970).

[14] See, e.g., Ref. 1, p. 329.

[15] R. Zhou, K.-A. Wang, Y. Wang, P. C. Eklund, M. S. Dresselhaus, and G. Dresselhaus, Phys. Rev. B **46**, 2595 (1992).

[16] M. M. Mitch, S. J. Chase, and J. S. Lannin, Phys. Rev. Lett. **68**, 883 (1992).

[17] See, e.g., M. B. Robin and P. Day, Adv. Inorg. Chem. Radiochem. **10**, 247 (1967); Y. Baer and W.-D. Schneider, in *Handbook on the Physics and Chemistry of Rare Earths*, edited by K. A. Gschneidner, Jr., L. Eyring, and S. Hüfner, (North-Holland, Amsterdam, 1987), Vol. 10.

[18] T. R. Ohno, G. H. Kroll, J. H. Weaver, L. P. F. Chibante, and R. E. Smalley, Phys. Rev. B **46**, 10 437 (1992).

[19] B. Xia, M. W. Ruckman, and M. Strongin, Phys. Rev. B **48**, 14 623 (1993).

[20] See, e.g., A. F. Wells, *Structural Inorganic Chemistry*, 3rd ed. (Oxford, New York, 1962).

[21] R. S. Ruoff, Y. Wang, and D. Tomanek, Chem. Phys. Lett. **203**, 438 (1993).

[22] This applies to most materials for electron energies greater than 100 eV, cf., M. P. Seah and W. A. Dench, Surf. Interface Anal. **1**, 2 (1979).

[23] See, e.g., W. J. Evans and T. A. Ulibarri, J. Am. Chem. Soc. **109**, 4292 (1987); W. J. Evans, L. A. Hughes, and T. P. Hanusa, Organometallics **5**, 1285 (1986).

[24] See, e.g., M. R. Spirlet, J. Rebizant, C. Apostolidis, and B. Kanellakopulos, Inorg. Chim. Acta **139**, 211 (1987).

[25] The Yb-C distances in Fig. 9 are calculated from x-ray diffraction results (Ref. 5), which are based on presumed undistorted C_{60} molecules. In distorted C_{60}, however, the many C atoms at distances greater than 2.8 Å from *T*-site cations are actually displaced from their ideal positions, leading to an even broader distribution of higher-NN Yb-C shells than those in Fig. 9. EXAFS from these shells destructively interfere, giving the observed high degree of selective disorder.

[26] F. Wudl, Acc. Chem. Res. **25**, 157 (1992).

[27] P. J. Fagan, J. C. Calabrese, and B. Malone, Acc. Chem. Res. **25**, 134 (1992).

[28] However, calculations for K_6C_{60} find small ionic displacements and C_{60} distortions; cf. Refs. 29 and 30.

[29] S. C. Erwin and M. R. Pederson, Phys. Rev. Lett. **67**, 1610 (1991).

[30] W. Andreoni, F. Gygi, and M. Parrinello, Phys. Rev. Lett. **68**, 823 (1992).

[31] R. Taylor and R. M. Walton, Nature (London) **363**, 685 (1993).

[32] C_{60} is not an aromatic molecule, but rather a collection of nested single-bonded pentagonal and double-bonded hexagonal rings, which are strained; cf. Ref. 1, p. 292, and Ref. 33.

[33] See, e.g., R. C. Haddon, Acc. Chem. Res. **25**, 127 (1992).

[34] The *p* faces have been called ''electron-poor'' in undoped, *neutral* C_{60} because the ''electron-rich'' double bonds of the *h* faces are oriented over the *p* faces at low temperatures; cf. Ref. 1, p. 184. This energetically weak ordering process should not be confused with the more energetic process of transferring externally supplied charge into the electronegative *p* faces, i.e., doping with electron donors makes the *p* faces of the now *negative* C_{60} anions ''electron rich.''

[35] Electronegative C_5H_5 rings are discussed in *The Feynman Lectures on Physics*, 3rd ed., edited by R. P. Feynman, R. B. Leighton, and M. Sands (Addison-Wesley, Reading, MA, 1966), Vol. 3, Chap. 15-5.

[36] See, e.g., S. Saito and A. Oshiyama, Phys. Rev. Lett. **66**, 2633 (1991).

[37] W. Andreoni, P. Giannozzi, and M. Parrinello, Phys. Rev. B **51**, 2087 (1995).

[38] A similar localization is found in the complex $\{[(C_2H_5)_3P]_2Pt]\}_6(\eta^2\text{-}C_{60})$, where six bridging bonds form across each of the six pyracylene units in C_{60}; cf. Ref. 27.

[39] In other parts of the complex there are changes in bond angle, but not bond lengths; cf. Ref. 33.

[40] R. Saito, G. Dresselhaus, and M. S. Dresselhaus, Chem. Phys. Lett. **210**, 159 (1993).

[41] See, e.g., Ref. 1, Chap. 8.

[42] S. Saito and A. Oshiyama, Solid State Commun. **83**, 107 (1992).

[43] S. C. Sockwell and T. P. Hanusa, Inorg. Chem. **29**, 76 (1990); R. A. Williams, T. P. Hanusa, and J. C. Huffman, Organometallics **9**, 1128 (1990).

[44] P. W. Stephens, L. Mihaly, P. L. Lee, R. Kaner, F. Deiderich, and K. Holczer, Nature (London) **351**, 632 (1991).

[45] A. R. Kortan, N. Kopylov, R. M. Fleming, O. Zhou, F. A. Thiel, R. C. Haddon, and K. M. Rabe, Phys. Rev. B **47**, 13 070 (1993).

[46] The experimental lattice constants in the A15 Ba_3C_{60} and fcc K_3C_{60} compounds were used in the calculations of Ref. 45.

[47] K. M. Rabe and P. H. Citrin (unpublished).

[48] Q. Zhu, O. Zhou, J. E. Fischer, A. R. McGhie, W. J. Romanow, R. M. Strongin, M. A. Cichy, and A. B. Smith III, Phys. Rev. B **47**, 13 948 (1993).

[49] M. J. Rosseinsky, D. W. Murphy, R. M. Fleming, R. Tycko, A. P. Ramirez, T. Siegrist, G. Dabbagh, and S. E. Barrett, Nature (London) **356**, 416 (1992).

[50] R. M. Fleming, A. P. Ramirez, M. J. Rosseinsky, D. W. Murphy, R. C. Haddon, S. M. Zahurak, and A. V. Makhija, Nature (London) **352**, 787 (1991).

[51] T. Yildirim, L. Barbedette, J. E. Fischer, C. L. Lin, J. Robert, P. Petit, and T. M. Palstra, Phys. Rev. Lett. **77**, 167 (1996).

[52] O. Zhou, J. E. Fischer, N. Coustel, S. Kycia, Q. Zhu, A. R. McGhie, W. J. Romanow, J. P. McCauley, Jr., A. B. Smith III, and D. E. Cox, Nature (London) **351**, 462 (1991).

[53] A. R. Kortan, N. Kopylov, S. Glarum, E. M. Gyorgy, A. P. Ramirez, R. M. Fleming, O. Zhou, F. A. Thiel, P. L. Trevor, and R. C. Haddon, Nature (London) **360**, 566 (1992).

[54] See Refs. 24, 34, 76, and 77 cited in Ref. 55.

[55] N. Nücker, E. Pellegrin, P. Schweiss, J. Fink, S. L. Molodtsov, C. T. Simmons, G. Kaindl, W. Frentrup, A. Erb, and G. Müller-Vogt, Phys. Rev. B **51**, 8529 (1995).

[56] H. Yoshikawa, S. Kuroshima, I. Hirosawa, K. Tanigaki, and J. Mizuki, Chem. Phys. Lett. **239**, 103 (1995).

[57] T. R. Ohno, Y. Chen, S. E. Harvey, G. H. Kroll, P. J. Benning, J. H. Weaver, L. P. F. Chibante, and R. E. Smalley, Phys. Rev. B **47**, 2389 (1993).

[58] A. R. Kortan (unpublished).
[59] Nominally trivalent La has been reported to exist in La_xC_{60} as a divalent cation; cf. C. Cepak, M. R. C. Hunt, A. Goldoni, S. Prato, and S. Modesti, in *Physics and Chemistry of Fullerenes and Derivatives*, edited by H. Kuzmany *et al.* (World Scientific, Singapore, 1995), p. 284.
[60] A. R. Kortan, N. Kopylov, E. Özdaş, A. P. Ramirez, R. M. Fleming, and R. C. Haddon, Chem. Phys. Lett. **223**, 501 (1994).
[61] X. H. Chen, X. J. Zhou, and S. Roth, Phys. Rev. B **54**, 3791 (1996).
[62] E. Özdaş, A. R. Kortan, N. Kopylov, A. P. Ramirez, T. Siegrist, and P. H. Citrin, in *Recent Advances in the Chemistry and Physics of Fullerenes and Related Materials: Volume 3*, edited by K. M. Kadish and R. S. Ruoff (Electrochemical Society Press, New Jersey, 1996), p. 1176.
[63] J. E. Fischer, G. B. Bendele, R. Dinnebier, P. W. Stephens, C. L. Lin, N. Bykovetz, and Q. Zhu, J. Phys. Chem. Solids **56**, 1445 (1995).
[64] I. Hirosawa, H. Kimura, J. Mizuki, and K. Tanigaki, Phys. Rev. B **51**, 3038 (1995).
[65] G. Nowitzke, G. Wortmann, H. Werner, and R. Schlögl, Phys. Rev. B **54**, 13 230 (1996).
[66] G. B. Bendele, P. W. Stephens, and J. E. Fischer, Phys. Rev. B (to be published).